Ceramics International **24** (1998) 379–386

PII: S0272-8842(97)00025-4
0272-8842/98 $19.00+.00

Failure of Silicon Nitride Rolling Elements with Ring Crack Defects

M. Hadfield*

Department of Product Design & Manufacture, Bournemouth University, 12 Christchurch Road, Bournemouth, Dorset BH1 3NA, UK

(Received 26 August 1996; accepted 12 January 1997)

Abstract: Hot isostatically pressed silicon nitride rolling elements are currently used in hybrid rolling element bearings. Surface defects such as ring cracks are difficult to detect during high volume production processes and hence there is a need to assess their influence on the rolling contact performance of the material. An accelerated rolling contact fatigue bench test is used to examine failure mode and performance of silicon nitride rolling elements with and without surface ring cracks. The surface ring cracks are found on silicon nitride as purchased from manufactures and are not produced artificially. Experimental test results are presented with pre-test surface analysis using a dye penetration technique. Theoretical calculations of the lubrication regime, contact stress fields and finite element analysis are presented. Scanning electron microscopy is employed to observe the failure modes of the silicon nitride rolling elements. © 1998 Elsevier Science Limited and Techna S.r.l. All rights reserved

1 INTRODUCTION

The use of specialist materials in surface engineering applied to rolling element bearings is needed to enable the design of components to increasingly higher performance specifications. Industries requiring high technological growth such as aerospace and energy supply require the use of rolling element bearings which operate within unconventional tribological and high temperature conditions respectively. In this present study a modified four-ball machine is used to produce accelerated contact failures on silicon nitride rolling elements with and without ring crack defects. Hot Isostatically Pressed (HIP) silicon nitride was used because of its practical availability and overall suitability of physical qualities for use in rolling element applications.

High quality engineering ceramics have been used in wear resistant applications for many years. This has enabled experience to be gained with regard to solutions where ceramics are suitable and economically advantageous. There has been a gradual improvement in the properties of advanced ceramics including the ultra-hard materials and reduction in cost, such that the promise of fully dense silicon nitride for bearing applications (noted for example by Scott[1] and Gielisse *et al.*[2]) has now been realised to the extent that ceramic ball bearings have been available commercially for some time. Quality control of the ceramic ball surfaces has reached a satisfactory position and high volume inspection is practical. Surface cracks were however occasionally found on ceramic balls,[3] hence research of their influence on fatigue failure modes was necessary. Ring cracks caused by manufacturing pressing faults or blunt impact loads are the most common type found on ceramic ball surfaces.

Circular surface cracks have been studied theoretically in the past by Hüber[4] and more recently by Li *et al.* [5] and Ueda.[6] Ueda also studied lateral and radial surface cracks, these are less common and occur due to poor sintering mixture and by sharp indention loads. A review paper by Warren *et al.*[7] discusses ring crack initiation and propagation using analytical techniques. The first two stages of surface defect growth showed that surface flaws develop into compete rings. In the final phase the crack develops into a cone. An experimental

study by Hadfield *et al.*[8] with artificially pre-cracked balls revealed the role played by a lubricating medium in the process of fatigue failure. The pre-cracks were formed by an impact indentation process in which fully developed cone cracks were formed and the rolling contact fatigue mode was spalling. In that study the artificially produced ring crack depth within the silicon nitride subsurface typically reached 20 μm before developing into a cone crack.

2 CONTACT FATIGUE TEST CONDITIONS

2.1 Test Machine

Accelerated rolling contact fatigue tests were performed using a modified four-ball machine (Fig. 1). This machine was employed as it correctly models ball-bearing motions and precisely defines the contact load. This machine consists of an assembly which simulates an angular contact ball-bearing. The stationary steel cup represents a bearing outer-race, three lower balls represent the rolling elements within a bearing-race and the upper ball represents the inner-race. The assembly was loaded via a piston below the steel cup, from a lever-arm load. The upper-ball was assembled to a drive shaft via a collet and contacts with three lower-balls when the machine is stationary. The contacting positions between the upper ball and lower balls were immersed with lubricating oil. The tests were suspended automatically at a set number of drive-shaft revolutions measured by a tachometer. A vibration sensor automatically stopped tests at a pre-determined potentiometer adjustment sensitivity (380) and light emitting diode duration. When the machine vibrates such that the diode remains in the on mode for more than 1 s the drive motor will cut out and the timer will stop. This machine can test materials and lubricants at shaft speeds between 100 and 20 000 r min^{-1}. All of the present tests were conducted at a shaft speed of 5000 r min^{-1}. The four-ball machine kinematics was presented by Tourret and Wright.[9]

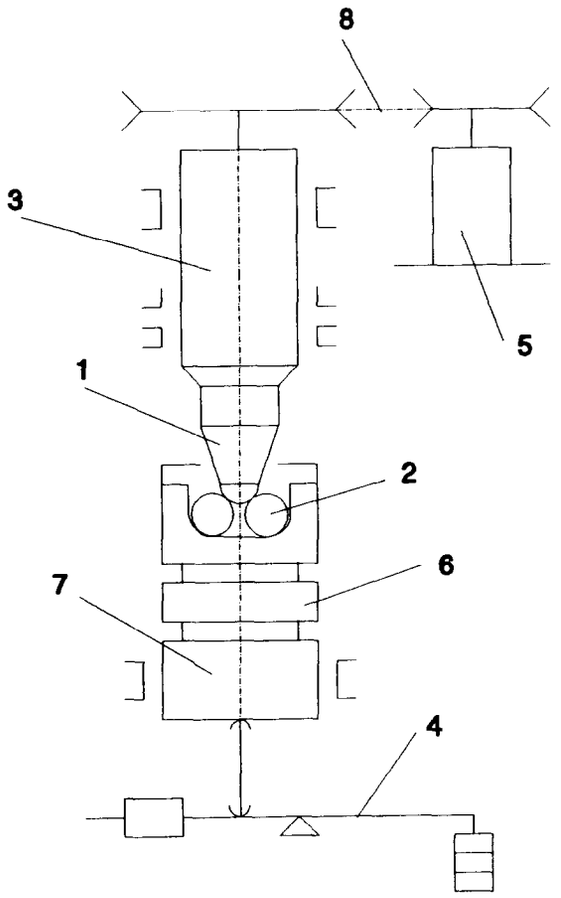

Fig. 1. Schematic of the modified four-ball machine. (1), Upper-ball and collet; (2) lower-balls; (3) spindle; (4) loading lever; (5) driving motor; (6) heated plate; (7) loading piston; (8) belt drive.

2.2 Test materials

The silicon nitride balls were manufactured by a Hot Isostatically Pressed (HIP) method. Ball blanks were ground and polished to 12.7 mm diameter, standardised procedures were adopted to ensure consistent quality of material and geometry. Average roughness (Ra) of the silicon nitride ball surfaces were 0.01 μm and ball roundness was within ball-bearing tolerances. Nominally perfect silicon nitride balls were used in test 'A' (Table 1). These balls were found to be fully dense and without surface ring cracks. The remaining tests 'B' to 'F' (Tables 1 and 2) were supplied from a different manufacturer. These were found to contain porosity and some ring crack defects. Ring crack defects were not found on balls used in test 'B', but were

Table 1. Fatigue tests 'A' and 'B'—without ring cracks at 5000 r min^{-1}; steel upper/silicon nitride lower

Test	A	B
Lever-arm load (kg)	10.0	5.0
Time to failure (s)	3400 (suspend)	4570
Lubricant	LV	LV
Final bulk temperature (°C)	43	51

Table 2. Fatigue tests 'C' to 'F'—with ring cracks at 5000 r min^{-1}; steel upper/silicon nitride lower

Test	C	D	E	F
Lever-arm load (kg)	10.0	5.0	10.0	5.0
Time to failure (s)	5300	5106	5553	4063
Lubricant	HV	HV	LV	LV
Final bulk temperature (°C)	52	44	56	46

found on the balls used in tests 'C' to 'F' The steel balls were grade 10 (ISO 3290-1975) carbon chromium steel with a surface roughness of 0.02 μm Ra.

Hardness of the test materials were measured using a Leitz Miniload 2 micro hardness tester. This tester can measure Vickers, Knoop and scratch hardness with various loads. In this case Vickers hardness was measured using a load of 500 p (4.903 N). The four-ball machine steel cup measured 756 Hv, and the steel balls were 839 Hv. The silicon nitride ball used in the qualifying test 'A' (Table 1) was 1832 Hv and the remaining balls which contained ring crack defects used in tests 'B' to 'F' were 1637 Hv.

Light microscopy was employed to examine the silicon nitride surfaces and characterise ring crack defects. A dye-penetrant method and microscopy using ultra-violet light source was utilised to enhance the detection of ring cracks and surface porosity. Figure 2 illustrates two examples of ring cracks found on the silicon nitride ball surfaces before testing. Figure 2(a) shows a white-light microscopic image of a silicon nitride ball surface, dark metallic phases are evident. The same area and magnification (Fig. 2(b)) is shown under ultra-violet light, now a ring crack of length 287 μm and diameter of 360 μm is evident. More serious damage is shown in Fig. 2(c) and (d). Again the ring cracks are only evident after dye-penetration treatment and shown under ultra-violet light. Five ring cracks can be seen in Fig. 2(d), the largest of 507 μm length and 514 μm diameter. It should also be noted that porosity can be seen on the surfaces in Fig. 2(b) and (d).

2.3 Lubrication regime

During testing, the upper-ball is lubricated from contact with the three planetary balls by a thin film of oil. The magnitude of separation between the surfaces and the lubrication regime is calculated using the classical ElastoHydroDynamic (EHD) eqn (1) developed by Hamrock and Dowson:[10]

$$H_{\min} = 3.63U^{0.68}G^{0.49}W^{-0.073}(1 - e^{-0.68K}) \qquad (1)$$

where U, G, W and K are dimensionless parameters for speed, materials, load and elipticity

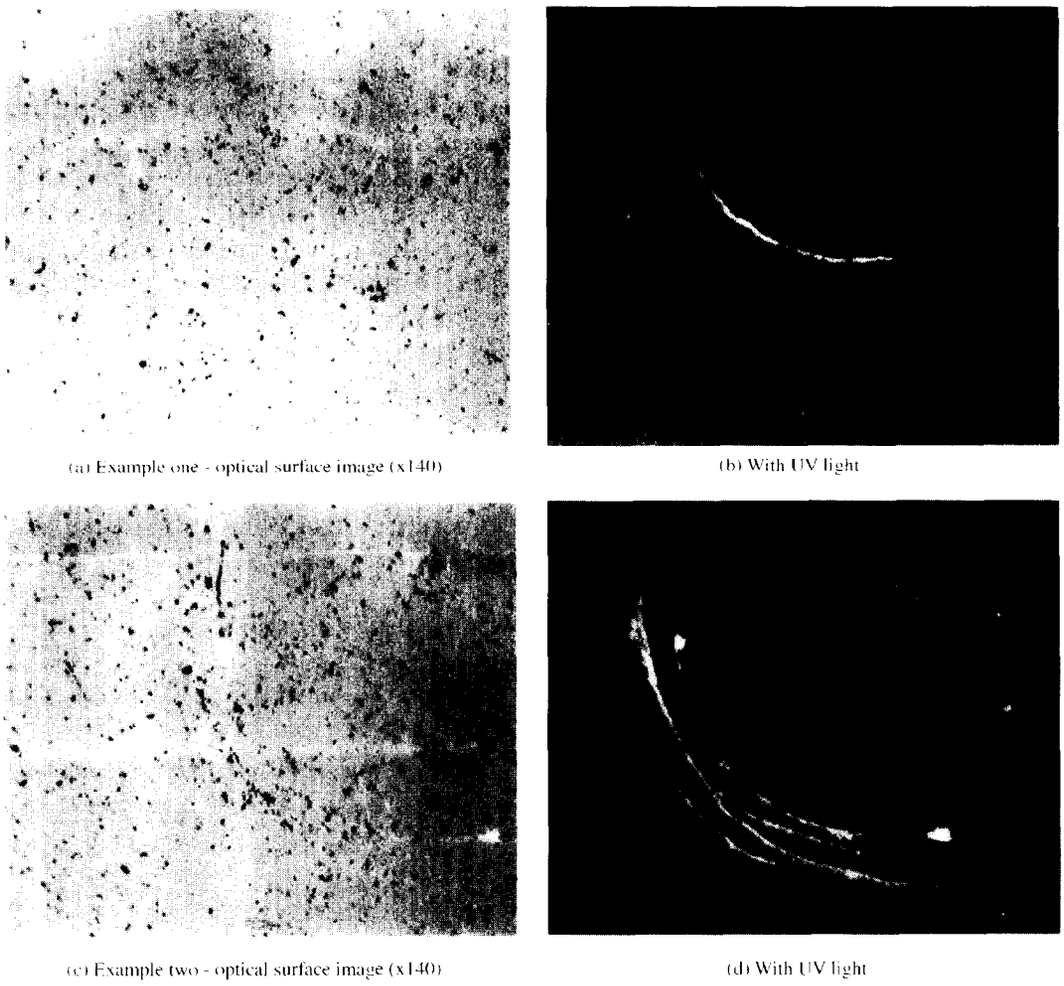

(a) Example one - optical surface image (x140) (b) With UV light

(c) Example two - optical surface image (x140) (d) With UV light

Fig. 2. Pre-test surface ring cracks on HIP silicon nitride balls: (a) example 1 optical surface image (×140); (b) with UV light: (c) example 2—optical surface image (×140); (d) with UV light.

respectively. The minimum film thickness (h_{min}) is found from the product of the dimensionless minimum film thickness parameter (H_{min}) and effective ball radius. At these conditions, thin film separation exists and stresses may be considered Hertzian. Oil Lubrication is designated (LV) for low viscosity oil and (HV) for high viscosity oil. The low viscosity lubricant is a synthetic oil which has a kinematic viscosity of 12.5 c.s.°C at 40°C and 3.2 c.s.°C at 100°C. The high viscosity lubricant is a mineral oil of 200 c.s.°C at 40°C and 40 c.s.°C at 100°C. The lubrication regime (lambda) is found from the ratio of minimum film thickness to composite surface roughness. Table 3 summarises the calculated minimum film thickness and lambda ratio for the upper-ball/lower-ball contacting surfaces. The most important finding from these calculations is that the lambda ratio for the LV lubricant is between one and three, this means that a 'mixed' EHD lubrication regime exists during testing at these conditions and hence some asperity contact will take place. In the case of the HV a lambda value of well above three is calculated and hence full separation exists and no asperity contact is envisaged.

2.4 Contact stress field

The contact stress field at the upper-ball/lower-ball interface is calculated using contact stress Hertz theory and presented in Table 4. This model is appropriate for lubrication outlined in Section 2.3. Rolling friction coefficient has been measured at less than 0.01 and therefore can be neglected for calculation purposes.[11] The contact load (P) is calculated using the lever-arm mass (M) and contact angle of 35.3° (θ) shown in eqn (2):

$$P = \frac{196.2\,M}{3\cos\theta} \tag{2}$$

Table 3. Calculated lubrication parameters

Test	Minimum film thickness H_{min} (nm)	Lambda ratio λ
A	54	2.4
B	57	2.6
C	294	13.1
D	309	13.8
E	54	2.4
F	57	2.6

Hertz contact equations[12] are used to calculate stress magnitudes, stress positions and contact circle size also found in Table 4. For a non-conforming spherical contact the maximum compressive stress (P_o) is given in eqn (3) where E_1 is an effective elasticity modulus for ceramic/steel contact and R_1 is an effective geometric radius. Equations for contact radius, shear/tensile stress and stress positions may be obtained in reference books, e.g. Ref. 13.

$$P_o\left(\frac{6PE_1^2}{\pi^3 R_1^2}\right) \tag{3}$$

A finite element model can also be utilised to study the contact stress field. Figure 3 shows the axisymmetric contact model and stress field resulting from a lever-arm load of 10 kg (tests 'A', 'C' and 'E'). This type of model is accurate for symmetrical problems where out of plane stains are insignificant; circumferential or 'hoop' strains are included. The mesh (Fig. 3(a)) contains 356 quadratic type elements. The contact model is restrained along the load the 'x' axis of symmetry in 'y' direction and along the 'y' axis in the 'x' direction. The solution is found iteratively by gradually increasing the contact area and thus including additional assigned nodes and coupling them together within the stiffness matrix until equilibrium is achieved. In this case the analysis converged after five iterations and contact radius 250 μm.

Figure 3(b) shows maximum principal shear stress contours. The left ball is ceramic and shows high concentration levels compared to the steel ball. The calculated contact radius of 195 and 240 μm for lever-arm loads of 5 and 10 kg, respectively, are of the same magnitude as the pre-test ring cracks described in Section 2.2. The maximum compressive stresses of 5.1 and 6.4 GPa are high compared with rolling element bearing operating conditions of around 3.0 GPa but are acceptable for accelerated fatigue testing.

2.5 Test program and results

2.5.1 Silicon nitride rolling elements without ring cracks

Tests 'A' and 'B' were each performed using three silicon nitride lower balls in contact with a steel

Table 4. Calculated contact stress

Lever-arm load (kg)	Contact load (N)	Contact radius (μm)	Maximum compressive stress (GPa)	Maximum shear stress (GPa)	Maxiumum shear stress depth (μm)	Maximum tensile stress (MPa)
5.0	400	195	5.1	1.6	96	675
10.0	800	240	6.4	2.0	121	860

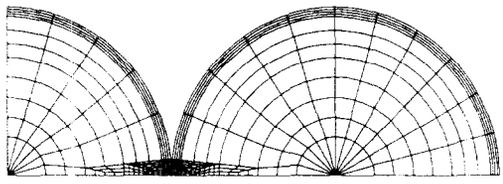

(a) Finite element mesh

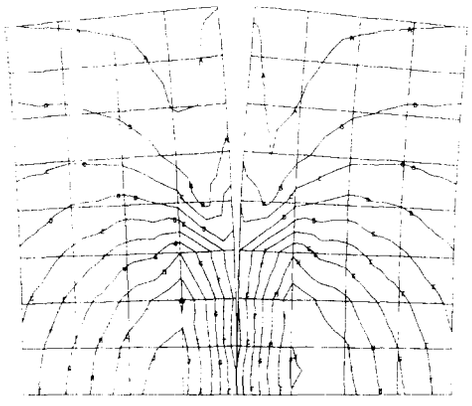

(b) Maximum shear stress GPa (one division = 100 μm)
A, 0.14; B, 0.35; C, 0.55; D, 0.76; E, 0.97; F, 1.17; G, 1.38; H, 1.59; I, 1.79; J, 2.0

Fig. 3. Finite element mesh and shear stress field (10 kg load): (a) finite element mesh; (b) maximum shear stress GPA (one division = 100 μm): A—0.14, B—0.35, C—0.55, D—0.76, E—0.97, F—1.17, G—1.38, H—1.59, I—1.79, J—2.0.

upper ball described in Table 1. Pre-test ring cracks were not found on any surface during this test program after extensive dye-penetration analysis. Both tests were performed using the low viscosity (LV) lubricant. Test 'A' was suspended after 3400 s with no increase in vibration during the test and debris were not present within the lubricant. Test 'B' was performed using a lower load and in this case the machine cut-out after 4570 s and ceramic powder-like ceramic debris were found within the lubricant. The bulk oil temperature gradually increased during both tests consistent with heat generated from material elastic hysteresis.

2.5.2 Silicon nitride rolling elements with ring cracks

Tests 'C' to 'F' were each performed using three silicon nitride lower balls where post-test ring cracks had been found and characterised. Two lubricants were used, High Viscosity (HV) and Low Viscosity (LV). The lever-arm load was also varied from 10 to 5 kg as designated in Table 2. Time to failure for all four tests did not vary significantly. During all tests powder ceramic debris were found within the lubricant. Again the oil bulk

(a) Overview of ball surface

(b) Wear scar and flaking failure

(c) Depth of flaking failure

Fig. 4. Post-test silicon nitride surface damage—test 'D': (a) overview of ball surface; (b) wear scar and flaking failure; (c) depth of flaking failure.

temperatures increased reflecting hysteresis friction losses.[14]

3 FAILURE ANALYSIS AND DISCUSSION

Silicon nitride rolling element test results shown in Table 1 indicate that premature failure occurs during test 'B'. Nominally perfect silicon nitride (test 'A') is suspended after running without failure and similar results have been reported[15] using the same material. The contrasting time to failure of tests 'A' and 'B' point towards failure which is unrelated to surface ring cracks. Similar times to failure are found when considering the test results from Table 2 on silicon nitride rolling elements with ring cracks. These failure times are also similar to test 'B' which again points towards failure which is unrelated to surface ring cracks. The lubrication regime for tests 'C' and 'D' is full separation EHD whilst for tests 'E' and 'F' it is mixed. No significant change of time to failure is found between the tests operating at different lubrication regimes, this indicates that although some asperity contact may take place, it does not appear to relate to material life performance at these test conditions.

Examples of ring cracks found silicon nitride ball surfaces in tests 'C' to 'F' are shown in Fig. 2 and described in Section 2.2. The dye-penetrant method was again used to examine the condition and possible subsurface growth of ring cracks on each ball after testing. After detailed examination under ultra-violet light microscopy no surface ring cracks were found on any post-test ball. Subsurface examination of post-test ring crack growth was therefore not possible. This leads to a hypothesis that the ring cracks were removed during testing.

Scanning electron micrographs of a silicon nitride post-test 'D' rolling element are shown as Fig. 4. The overview of the ball surface (Fig. 4(a)) shows extensive and severe wear. This type of wear is three-body abrasion due to the direct wear scars (Fig. 4(b)), the evidence of fine ceramic debris within the lubricant and the full film lubrication regime indicated in Table 3. Some evidence of flaking failure can also be seen in Fig. 4(b) which inclosed the direct wear path (scratches) between

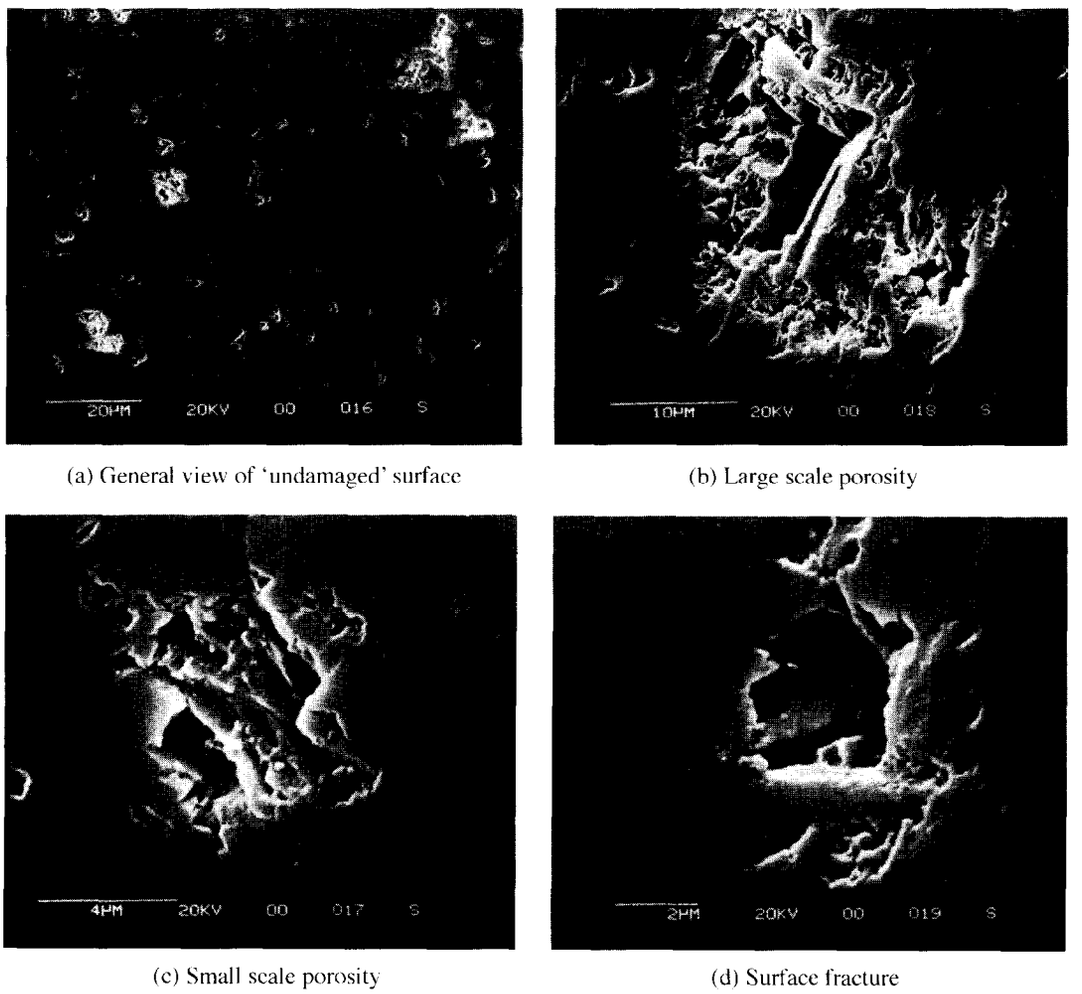

(a) General view of 'undamaged' surface

(b) Large scale porosity

(c) Small scale porosity

(d) Surface fracture

Fig. 5. Silicon nitride porosity—test 'D': (a) general view of 'undamaged' surface; (b) large scale porosity; (c) small scale porosity; (d) surface fracture.

the upper and lower ball. The flaking type failure is quite shallow varying between 1 and 5 μm and can be visualised in Fig. 4(c). The depth of the flaking failure also indicates the original ring crack depth. As all evidence of the pre-test ring cracks is removed it is postulated that the maximum ring crack depth does not exceed 5 μm. It is therefore concluded that the pre-test ring cracks did not reach a depth at which a conical shape occurs i.e. at approximately 20 μm reported in Section 2.2. The depth at which the ring crack becomes critical in relation to the failure mode is unclear although a previous study testing[8] reported spalling failure due to cone crack and thus a depth of between 5 to 20 μm is realistic. Depth of maximum shear stress (Table 4 and Fig. 3) is 121 μm below the silicon nitride surface and therefore not related to the flaking depth.

Figure 5 shows evidence of ball 'D' porosity within an apparent undamaged area. The general view (Fig. 5(a)) illustrates extensive surface porosity which confirms the pre-test surface analysis described in Section 2.2. The scale of the porosity can by seen in Fig. 5(b) and (c) to vary from typically 300 to 50 μm^2. High magnification provides evidence of surface fracture and debris removal within porosity areas is also illustrated in Fig. 5(d). Crack lengths of 2 μm surrounding bulk material and radial cracks of 3 μm are evident. It is clear from Fig. 5 that debris removal can occur at areas that wear scars and flaking failure are not observed. It is possible that mechanism of initial debris removal from the silicon nitride rolling elements initiate from hydrostatic oil pressures within full film lubrication at porous areas. After the debris are removed from the porous areas then three body abrasive wear takes place. It should be noted that debris size indicated from Fig. 5(d) is approximately 2 μm diameter whereas the lubricant film thickness is only 0.3 μm. The role of the surface ring crack on the wear mechanism is unclear. In this case the shallow ring cracks extending no more than 5 μm within the ceramic material have been removed by abrasive wear and have not initiated any form of spalling failure. It should also be noted that the silicon nitride rolling elements used

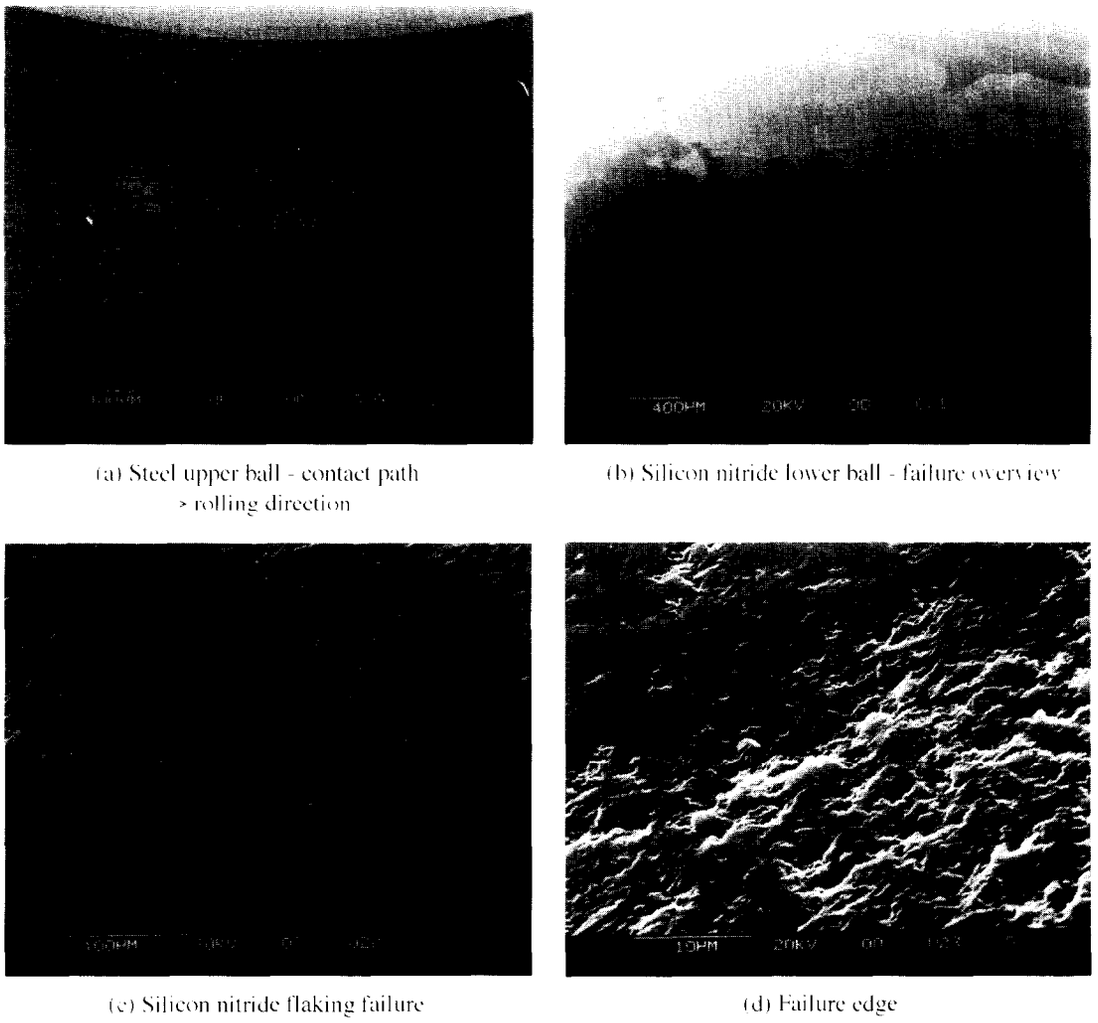

(a) Steel upper ball - contact path → rolling direction

(b) Silicon nitride lower ball - failure overview

(c) Silicon nitride flaking failure

(d) Failure edge

Fig. 6. Post-test steel and silicon nitride surface damage—test 'F': (a) steel upper ball—contact path (→ rolling direction); (b) silicon nitride lower ball—failure overview; (c) silicon nitride flaking failure; (d) failure edge.

in tests 'B' to 'F' have reduced hardness. This fact may also contribute to the failure.

Scanning electron micrographs of test 'F' steel upper-ball and silicon nitride lower-ball are shown as Fig. 6. This test was performed using the low viscosity (LV) lubricant at 5.1 GPa maximum compressive stress. The steel upper ball contact path (Fig. 6(a)) indicates extensive wear and wear path width of 1.01 mm which exceeds the theoretical unworn width of 0.39 mm (Table 2). Examination of the contact path edge and centre did not produce evidence of surface cracks. Plastic deformation of the steel upper-ball was not evident on the surface. This type of wear is expected on the steel upper ball considering the greater hardness of the ceramic and fine ceramic debris found within the lubricant. A silicon nitride lower-ball from test 'F' (Fig. 6(b)) shows a flaking failure similar to test 'D' although direct contact wear is not evident. Figure 6(c) shows an overview of the surface flaking failure, direct contact wear compared with Fig. 4(b) is not evident. Again, post-test ring cracks were not found. The interface of the shallow flaking failure and evidence of porosity is shown as Fig. 7(d). The absence of direct contact wear may be a result of smaller debris produced by asperity contact during the initial stages of testing whereas asperity contact is not expected using the HV lubricant.

4 CONCLUSIONS

The failure mode or life of silicon nitride rolling elements was not related to the presence of surface ring crack defects at these test conditions. Porosity is the dominant property which controls wear mode and performance. The critical depth of the ring crack defect is 5 to 20 μm below the surface.

REFERENCES

1. SCOTT, D. & BLACKWELL, J., Hot pressed silicon nitride as a rolling bearing material—a preliminary assessment. *Wear*, **24** (1973) 61–67.
2. GIELISSE, P. J., WILSON, M. P., BORASE, V. N., HEUNG, L. K. & KIEHLE, A. J., *Ceramic materials for high temperature gas bearings*. Report on ONR Contract No. N00014-68-0215-008, Sept. 1972.
3. CUNDILL, R. T., *Rolling element bearings into the 21st century*. IMechE Seminar, London, Nov. 1990.
4. HÜBER, M. T., Zur theorie dc Beruhrung fester elastische Korper. *Ann. der Physics*, **14** (1904) 153.
5. YINGZHI, LI. & HILLS, D. A., The Hertzian cone crack. *Trans. of the ASME*, **58** (1991) 120–127.
6. UEDA, K., Contact-stress deformation and fracture in ceramics. *Jap. J. Tribology*, **34**(2) (1989) 123–131.
7. WARREN, P. D., HILLS, D. A. & DAI, D. N., Mechanics of Hertzian cracking. *Tribology Int.*, **28**(6) (1995) 357–362.
8. HADFIELD, M., STOLARSKI, T. A., CUNDILL, R. T. & HORTON, S., Failure modes of ceramic elements with ring crack defects. *Tribology Int.*, **26** (1992) 157–164.
9. TOURRET, R. & WRIGHT, E. P., Rolling contact fatigue: performance testing of lubricants. International Symposium, Institute of Petroleum, Oct. 1976.
10. JACOBSON, B. O., *Rheology and Elastohydrodynamic Lubrication*. Baker and Taylor, Elsevier, Amsterdam, 1991.
11. Engineering Sciences Data, No. 84017, Contact phenomena. 2: stress field and failure criteria in concentrated elastic contacts under combined normal and tangential loading, Oct. 1984.
12. HERTZ, H., On the contact of elastic solids. *J. Reine Angew Math.*, **92** (1881) 156–171.
13. JOHNSON, K. L., *Contact Mechanics*. Cambridge University Press, UK, 1985.
14. TABOR, D., The mechanism of rolling contact II. The elastic range. *Roy. Soc. Proc.: Ser. A*, **229** (1955) 198–220.
15. HADFIELD, M., STOLARSKI, T. A. & CUNDILL, R. T., Failure modes of ceramics in rolling contact. *Roy. Soc. Proc.: Ser. A*, **443** (1993) 607–621.